Monatshefte für Chemie 135, 519–541 (2004)
DOI 10.1007/s00706-003-0157-3

Monatshefte für Chemie
Chemical Monthly
Printed in Austria

Novel Linear Tetrapyrroles: Hydrogen Bonding in Diacetylenic Bilirubins

Bin Tu, Brahmananda Ghosh, and **David A. Lightner***

Department of Chemistry, University of Nevada, Reno, Nevada 89557, USA

Received November 24, 2003; accepted December 3, 2003
Published online March 18, 2004

Summary. Bilirubin congeners with dipyrrinones conjoined to a diaceteylene unit (–C≡C–C≡C–) rather than to $-CH_2-$ were synthesized and examined spectroscopically. This new class of rubrified linear tetrapyrroles cannot easily fold or bend in the middle, but the dipyrrinones can rotate independently about the diacetylene unit. Thus, unlike bilirubin, which is bent in the middle and has a ridge-tile shape, the diacetylene unit orients the attached dipyrrinones along a linear path, and intramolecular hydrogen bonding between the dipyrrinones and opposing carboxylic acids preserves a *twisted linear molecular shape* when the usual propionic acids are replaced by hexanoic. In a bis-hexanoic acid rubin, the extended planes of the dipyrrinones intersect along the $-(C\equiv C)_2-$ axis at an angle of 102° for the conformation stabilized by intramolecular hydrogen bonding. With propionic acid chains, however, neither CO_2H can engage an opposing dipyrrinone in intramolecular hydrogen bonding, and the energy-minimum conformation of this linear pigment, shows nearly co-planar dipyrrinones, with an intersection of an angle of ~180° of the extended planes of the dipyrrinones. Spectroscopic evidence for such linearized and twisted (bis-hexanoic) and planar (bis-propionic) structures comes from the pigments' NMR spectral data and their exciton UV-Vis and induced circular dichroism spectra.

Keywords. Pyrrole; Hydrogen bonding; Conformational analysis.

Introduction

Bilirubin, the neurotoxic yellow pigment of jaundice [1], and its biogenetic precursor (blue-green) biliverdin are formed copiously in healthy mammals by catabolism of hemoglobin and other heme proteins (Fig. 1A) [1, 3]. Both of these bile pigments are members of a class of compounds called ''linear tetrapyrroles'' [3], as distinct from cyclic tetrapyrroles, such as porphyrins, but are the structures really linear? *Fischer* determined their constitutional structures by degradation and total synthesis in 1941 and indicated linear structure representations, with lactim rather than lactam end rings and without designating the configurational stereochemistry of the C(4) and C(15) double bonds and (in biliverdin) the C(10) double bond [4].

* Corresponding author. E-mail: lightner@scs.unr.edu

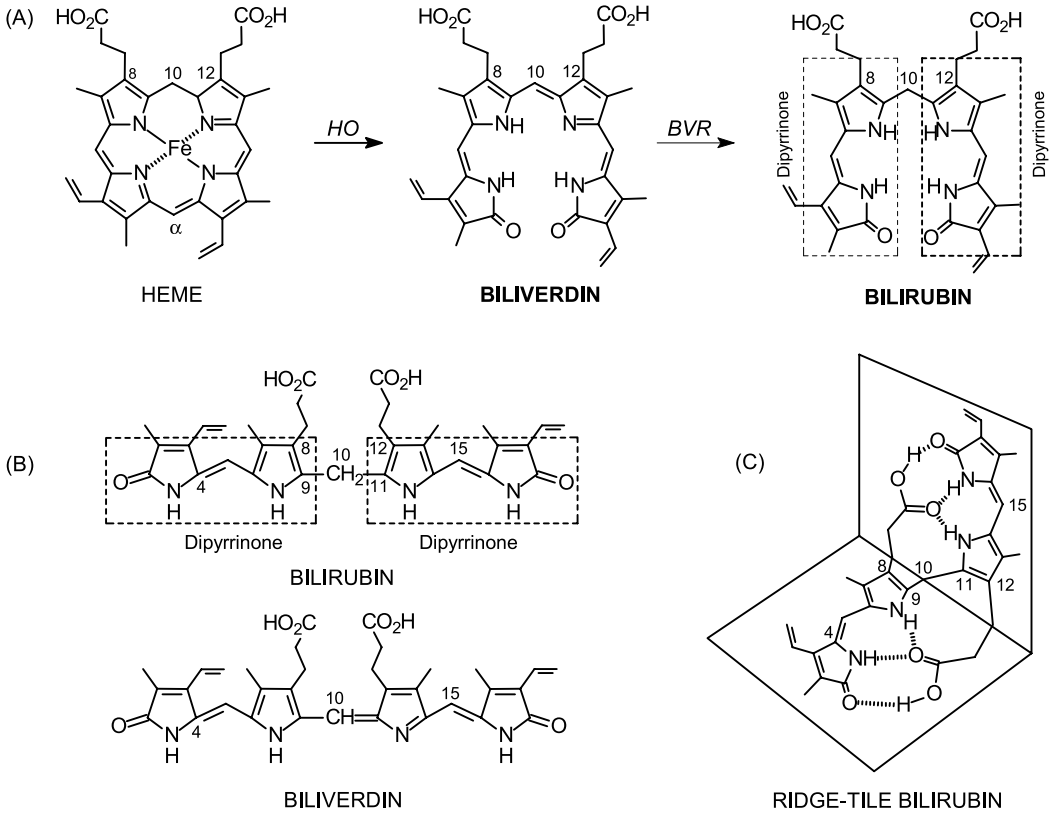

Fig. 1. (A) Formation of bilirubin and biliverdin from heme, *HO* = Heme Oxygenase; *BVR* = Biliverdin Reductase; (B) linear representations of bilirubin and biliverdin; the most stable conformation of biliverdin is porphyrin-like (as in A) and helical; the most stable conformation of bilirubin is neither linear nor porphyrin-like but shaped like a ridge-tile (C), and stabilized by intramolecular hydrogen bonding

Earlier, however, *Lemberg* [5] suggested that the 4*Z*, 10*Z*, and 15*Z* double bond configurations should follow logically from those of the porphyrin precursor, but with stated misgivings used ''linear'' representations [6]. Since *Fischer*, linear structures for bilirubin and biliverdin (Fig. 1B) have become common, and in most biochemistry texts the structures typically have the wrong (*E*) double bond stereochemistry, often with lactim end rings. Yet, both the *Z*-stereochemistry [3] and the lactam tautomer [3, 7] were shown to be more stable long ago. (4*Z*, 15*Z*)-Rubins and (4*Z*, 10*Z*, 15*Z*)-verdins are bent in the middle [8, 9]. The latter adopt a porphyrin-like conformation [3], but the former (whose dipyrrinones may in principle rotate freely about the central 10-CH_2) fold into a ridge-tile shape (Fig. 1C) stabilized by intramolecular hydrogen bonding between the propionic acids and the opposing dipyrrinones [9].

Verdins and rubins are bent in the middle, a stereochemistry that follows as a consequence of trigonal and tetrahedral hybridization, respectively, at C(10). A more truly ''linear'' tetrapyrrole would have digonal (or sp) hybridization at C(10), thus implying at least one –C≡C– group. Yet little is known of 10-homologated rubins, and most known examples are not necessarily constrained

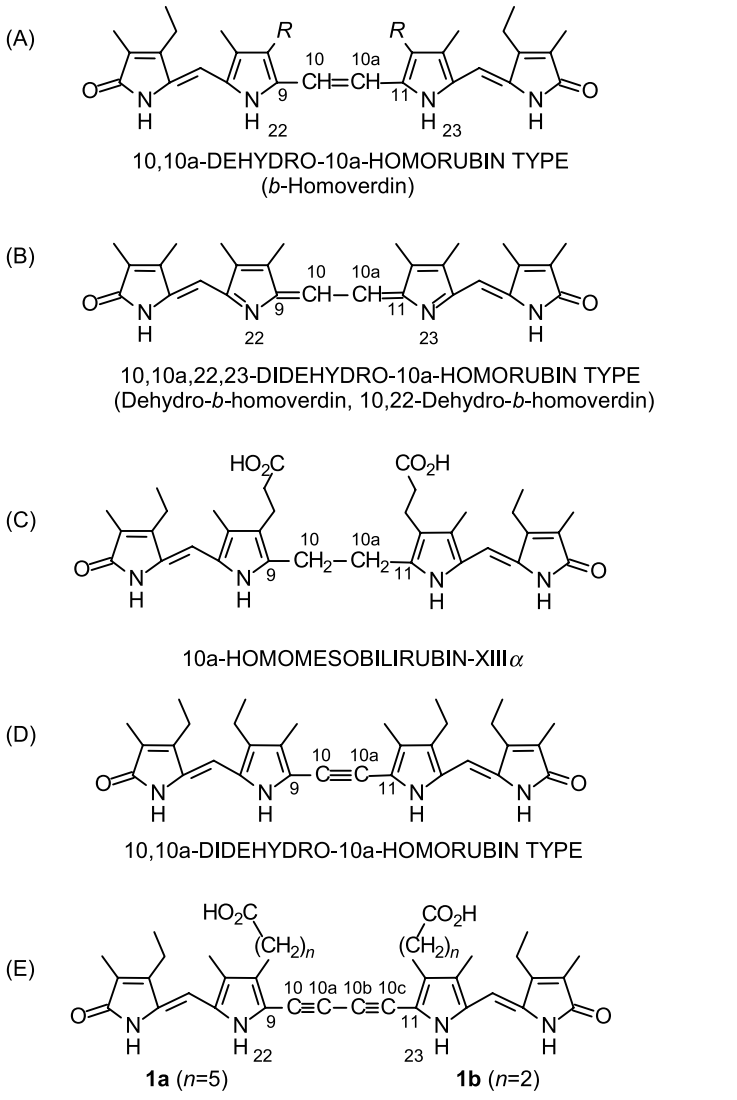

Fig. 2. (A) and (B) The homorubin/homoverdin types prepared in Refs. [10, 11], where in (A) $R = CH_2CH_2CO_2CH_3$ or $CH_2CO_2CH_3$ or CH_2CH_3; (C) the only known homorubin; (D) the isoelectronic, acetylene tautomeric analog of (B), see Ref. [12]; (E) the target diacetylene-rubins of this work

by hybridization to be linear. *Falk et al*. [10] first published on a new class of (red) dehydro-10a-homorubins (Fig. 2A), also called *b*-homoverdins, and a didehydro-10a-homorubin or dehydro-*b*-homoverdin (also red) (Fig. 2B), was also prepared. At about the same time, we published on the first (yellow) 10a-homorubin (Fig. 2C) [11]. Such tetrapyrroles are bent in the middle. Though a (10*E*)-*b*-homoverdin or (9*E*,10a*E*)-dehydro-*b*-homoverdin might assume a more or less linear shape, 10a-homorubins have more degrees of freedom about the C_9–C_{10}–C_{10a}–C_{11} segment, and thus 10a-homomesobilirubin-XIIIα is bent in the middle and intramolecularly hydrogen bonded.

In recent studies [12], we failed in attempts to synthesize an acetylenic etiobilirubin analog, with alkyl 10,10a-didehydro-10a-homorubin (Fig. 2D) that is isoelectronic and tautomeric with 10,10a,22,23-didehydro-10a-homorubin (Fig. 2B, dehydro-*b*-homoverdin). However, we were able to prepare the corresponding diacetylene analog, the first of a new class of linear tetrapyrroles [12]. Given our success synthesizing diacetylene rubins, in the following, we describe the synthesis, conformation, and spectroscopic properties of the first *intramolecularly hydrogen-bonded* linear bilirubin analog (**1a**) with the 10-CH_2 group replaced by a –C≡C–C≡C– (Fig. 2E). Molecular models indicate that such novel rubins possessing hexanoic acids (**1a**) at C(8) and C(12) can engage in intramolecular hydrogen bonding, with the CO_2H groups fitting nicely into a bilirubin-like (Fig. 1C) intramolecular hydrogen bonding motif by engaging the dipyrrinones. However, with propionic acids (**1b**), the acid chains are too short to permit either CO_2H to engage in such intramolecular hydrogen bonding. Thus, both **1a** and **1b** serve as useful comparative models for analyses of linear and linearly conformationally-arrested bilirubins.

Results and Discussion

Synthesis Aspects

Based on our experience in synthesizing the first per-alkylated diacetylenic rubin [12], we surmised that the simplest route to the preparation of acetylenic rubins **1a** and **1b** would be the "1 + 2 + 1" approach [13] outlined in Scheme 1. In Scheme 1, an α,α'-diformyldipyrrolyldiacetylene (**3a** or **3b**) is coupled with two equivalents of tosyl-pyrrolinone **4**. The required tosyl-pyrrolinone had been reported previously [14], but the required dipyrrole diacetylenes (**2a** and **2b**) were unknown. Dipyrrole diacetylenes **3a** and **3b** were prepared by coupling their respective monopyrrole mono-acetylenes (**5a** and **5b**), both of which were prepared from their respective iodopyrroles, **7a** and **7b**, both previously unreported. The precursors to **7b**, namely **10b** [15] and **11b** [16], were known from work in our laboratory; however, the corresponding precursors to **7a** (which are **10a** and **11a**) had not been reported, nor had the precursor diketo-ester **12a**, whose analog (**12b**) was used in the preparation of **11b** [16].

Diketo-ester **12a** was prepared from diethyl adipate (**15**) as outlined in Scheme 1 by reaction with one equivalent of KOH to give the mono-ester mono-potassium salt **14**, which was converted to mono-acid chloride **13** by treatment with oxalyl chloride. Acylation of the *TMS* enol ether of 2-butanone afforded **12a**, which was condensed with diethyl oximinomalonate in the presence of Zn and acetic acid via a *Fischer-Knorr* type reaction to afford pyrrole **11a** in an overall 17% yield. Similarly, the ethyl ester-acid chloride of succinic acid was converted to **10b** and carried forward to yield pyrrole **11b**. Oxidation of the α-methyl of **11** to α-formyl using *CAN* [17] gave **10** in 75% (**10a**) and 82% (**10b**) [15] yields. Iodine was introduced at the opposite α'-position first by saponification of the α'-ester of **10** using $LiOH \cdot H_2O$ at 70°C in aq. *THF* to give **9a** from **10a** and **9b** from **10b**, then by treatment with I_2-KI in aqueous bicarbonate to afford **8a** and **8b** in 23% yield. After esterification of the hexanoic (**8a**) and propionic (**8b**) acids with CH_2N_2, the

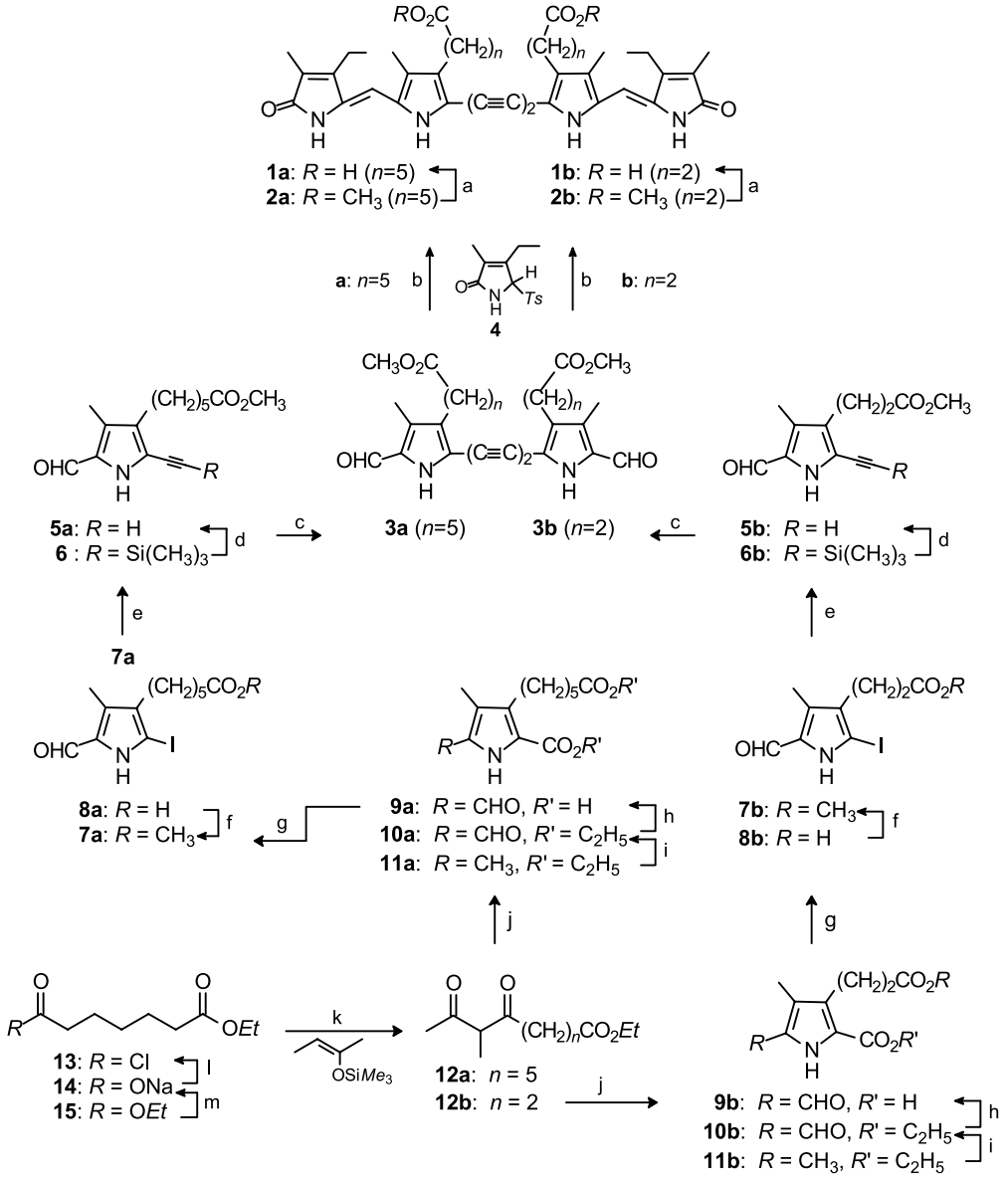

a: KOH, then HO*Ac*; b: *DBU*, *n-Bu*$_3$P; c: Pd(P*Ph*$_3$)$_4$, CuI, CH_3COCH_2Cl, dry C_6H_6, RT, 16 h; d: *n-Bu*$_4$NF, *THF*, RT; e: Pd(P*Ph*$_3$)$_2Cl_2$, CuI, HC≡C-*TMS*, *Et*$_2$NH, 50°C; f: CH_2N_2, CH_3OH; g: I_2, KI, $KHCO_3$, H_2O; h: $LiOH \cdot H_2O$, *THF*/H_2O, 70°C; i: *CAN*; j: HON=C(CO$_2$*Et*)$_2$, Zn, HO*Ac*; k: $ZnCl_2$, CH_2Cl_2; l: $(COCl)_2$; m: KOH.

Scheme 1

α'-iodine was replaced (in **7**) with *TMS*-acetylene in 75% yield by a *Sonagashira* reaction [18] using Pd(P*Ph*$_3$)$_2Cl_2$–CuI catalyst in *Et*$_2$NH. The resulting pyrrole acetylenes (**6a** and **6b**), obtained in 85% yield, were desilylated using *n-Bu*$_4$NF to provide **5a** and **5b**, which were then self-coupled in 65% yield using Pd(P*Ph*$_3$)$_4$

catalyst in the presence of chloroacetone, to afford the required α,α'-diformyldipyrrolyl-diacetylenes, **3a** and **3b**. Reaction of **3a** and **3b** with 4–5 mole equivalents of pyrrolinone **4** using *DBU* and tri-*n*-butylphosphine as catalyst gave the desired (red) acetylenic rubin esters **2a** and **2b** in good yield. Saponification of **2b** led smoothly to **1b**, but similar treatment of **2a** gave a product mixture from which **1a** could not be easily separated. It was isolated by subjecting the saponification product mixture to aq. KOH followed by acidification of the potassium salt with *Ac*OH, which precipitated **1a**.

Constitutional Structure

The constitutional structures of **1a** and **1b** follow from the method of synthesis (Scheme 1) and from their ^{13}C NMR spectra (Table 1). The ^{13}C NMR spectra of **1a**

Table 1. Comparison of ^{13}C NMR chemical shift assignments for planar bilirubin analogs **1a** ($X =$ –C≡C–C≡C–, $n = 5$) and **1b** ($X =$ –C≡C–C≡C–, $n = 2$) with mesobilirubin-XIIIα (*MBR-XIII*) ($X =$ –CH_2–, $n = 2$) in $(CD_3)_2SO$ (Chemical shifts in δ (ppm) downfield from $(CH_3)_4Si$)

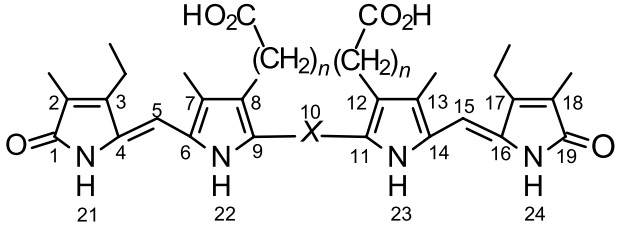

Position	**1a**	**1b**	*MBR-XIII*
2,18	124.8	125.3	122.5
2,18–CH_3	9.09	9.48	9.14
1,19–CO	172.1	172.5	171.8
3,17	147.3	147.8	147.2
3,17–*CH_2*CH_3	17.06	17.5	17.15
3,17–CH_2*CH_3*	14.67	15.1	14.81
4,16	132.7	132.3	127.8
5,15–CH=	95.6	96.0	97.69
6,14	126.8	127.3	122.0
7,13	121.5	122.1	122.9
7,13–CH_3	8.09	8.53	8.07
8,12	131.6	131.6	119.2
8^1–CH_2	24.3	20.8	19.25
8^2–CH_2	24.4	34.8	34.34
8^3–CH_2	28.2	–	–
8^4–CH_2	29.7	–	–
8^5–CH_2	33.5	–	–
8,12–COOH	174.4	174.0	174.0
9,11	112.1	112.4	130.3
10	80.1	80.8	23.46
10′	78.2	78.4	–

and **1b** are nearly identical except for the different number of carbons in the alkanoic acid chains. When compared with ^{13}C NMR data [19] from the known mesobilirubin-XIIIα (*MBR-XIII*), the various carbons of the dipyrrinone(s) of **1a** and **1b** have counterparts with recognizably similar chemical shifts. The C(10) signals of **1a** and **1b** are quite different from that of *MBR-XIII*, reflecting the replacement of $-CH_2-$ by $-C{\equiv}C-C{\equiv}C-$. Noticeable differences are also found at some ring carbons: C(9, 11) is ~18 ppm more shielded in **1a**/**1b** than in *MBR-XIII*, while C(18, 12) is ~12 ppm more shielded in **1a**/**1b** than in *MBR-XIII*. Far smaller differences (~2–5 ppm relative deshieldings) in **1a**/**1b** relative to *MBR-XIII* are found at C(2, 18), C(4, 16), and C(6, 14) that alternate along pathway of conjugated C=C bonds, while C(5, 15) is ~1 ppm more shielded.

Solution and Chromatographic Properties

In bilirubin and mesobilirubin-XIIIα, propionic acid chains enjoy optimal intramolecular hydrogen bonding (Fig. 1C) [8], but butyric acid chains are also found to possess the right geometry for engaging the dipyrrinones in hydrogen bonding [20, 21]. When the bilirubin acid chains are as short as acetic or as long as pentanoic and hexanoic, counter-intuitively the pigment polarity increases [21]. Generally, when the acid chain lengths are mismatched for effective intramolecular hydrogen bonding, as in bilirubins with pentanoic through octanoic acids at C(8) and C(12), the pigments typically exhibit increased polarity (on TLC and HPLC), decreased solubility in $CHCl_3$, and increased solubility in dilute aqueous bicarbonate.

Unlike their bright yellow parent, *MBR-XIII*, diacetylenic rubins **1a** and **1b** are red solids that form orange solutions. Analog **1b** is insoluble in most organic solvents such as $CHCl_3$, CH_2Cl_2, and CH_3OH. In contrast, **1a** exhibits limited solubility in $CHCl_3$ and CH_2Cl_2, an indication that **1a** is less polar than **1b**. Consistent with such polarity, on silica gel TLC using 4% by vol. CH_3OH in CH_2Cl_2 as eluent, **1a** has an $R_f \sim 0.45$, and **1b** has an $R_f \sim 0.0$, conditions where *MBR-XIII* exhibits an $R_f \sim 0.85$. The retention times on reverse phase HPLC are also consistent with the polarity difference: **1a** (14.3 min) lies between that of **1b** (7.2 min) and *MBR-XIII* (18.3 min). As with bilirubin and *MBR-XIII*, **1a** is not extracted into 5% (or saturated) aqueous sodium bicarbonate from chloroform; however, **1b** is extracted. Clearly, replacing the central $-CH_2-$ of *MBR-XIII* by $-C{\equiv}C-C{\equiv}C-$ has a major impact on the chloroform/bicarbonate partition coefficient of **1b**, but it does not have a large effect when the chain lengths are extended to hexanoic (**1a**). Taken collectively, these data suggest the presence of intramolecular hydrogen bonding in **1a**, but not in **1b**, as predicted by *CPK* molecular models, and as designed.

Intramolecular Hydrogen Bonding

The sp carbons of the acetylene unit guarantee a linear pigment geometry, with any bending in the middle coming from limited bending of the C(9)–C(10)–C(10a), C(10)–C(10a)–C(10b), C(10a)–C(10b)–C(10c), or C(10b)–C(10c)–C(11) bond angles, or within the dipyrrinones, principally from rotations about the C(4)–C(5)–C(6)–N(22) and N(23)–C(13)–C(14)–C(15) torsion angles, around the sp^2

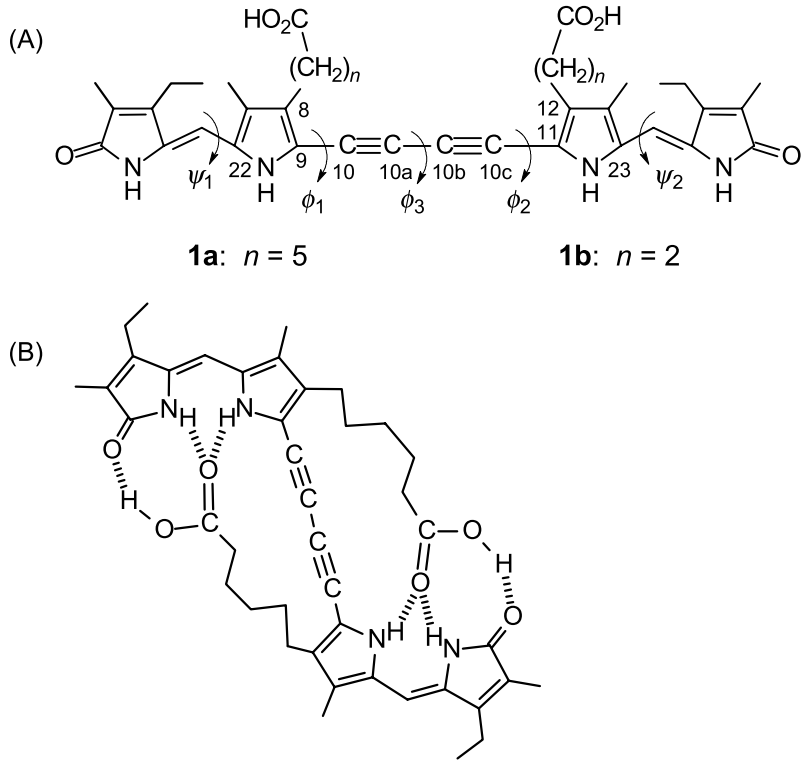

Fig. 3. (A) Linear representation of rubins **1a**–**1d**, with the usual central CH_2 of bilirubin replaced by a diacetylene unit; rotations about torsion angles ϕ_1, ϕ_2, and ϕ_3 interconvert the major important conformations; (B) Intramolecularly hydrogen-bonded representations of diacetylenic bilirubin analog **1a** with hexanoic acids replacing the usual propionic; the propionic acid chains of **1b** are too short to permit the (typical) sort of intramolecular hydrogen bonding shown; hydrogen bonds are shown by hatched lines

carbons 5 and 15. Like bilirubins [9], the dipyrrinone units of **1a** and **1b** may rotate freely and independently about torsion angles ϕ_1, ϕ_2, and ϕ_3 (Fig. 3A), about the two acetylenes, thereby leading to numerous rotational isomers. In some conformations, one or both dipyrrinones may be brought into sufficiently close proximity for intramolecular hydrogen-bonding to the carboxylic acid groups, given sufficient length of the alkanoic acid chain. For the diacetylene rubins, the propionic acids of **1b** are too short, but at least partial intramolecular hydrogen bonding becomes possible with longer chains. For fully engaged hydrogen bonding, the ideal minimum chain length seems to be that of hexanoic acid (Fig. 3B).

Consistent with the predictions based on acid chain length, **1a** is found to be sufficiently soluble in $CHCl_3$ for ^1H NMR measurements, but **1b** was insoluble. The ^1H NMR spectrum of **1a** reveals dipyrrinone NH chemical shifts (Table 2) essentially identical to those found in *MBR-XIII* in $CDCl_3$ [9, 19, 22] and characteristic of intramolecular hydrogen bonding to a carboxylic acid. Dipyrrinones are known to be avid participants in hydrogen bonding, preferably to carboxylic acids [23, 24], and secondarily to each other (with association constants $\sim 30000\, M^{-1}$ in $CDCl_3$) [25]. In $CDCl_3$, dipyrrinone monomers exhibit lactam

Table 2. Comparison of the lactam and pyrrole NH chemical shifts[a] of the diacetylenic tetrapyrroles **1a** and **1b** with mesobilirubin-XIIIα (*MBR-XIII*) in $CDCl_3$ and $(CD_3)_2SO$ solvents

Pigments	$CDCl_3$			$(CD_3)_2SO$		
	Lactam NH	Pyrrole NH	COOH	Lactam NH	Pyrrole NH	COOH
1a	10.54	9.26	13.08	9.90	11.16	11.96
1b	–	–	–	9.86	11.19	12.07
MBR-XIII	10.57	9.15	13.62	9.72	10.27	11.87

[a] δ, in ppm downfield from $(CH_3)_4Si$

and pyrrole NH chemical shifts of ~8 ppm [25b], but intermolecularly hydrogen-bonded dipyrrinone dimers typically exhibit lactam and pyrrole NH chemical shifts ~11 and ~10 ppm, respectively. Dipyrrinones hydrogen bonded to CO_2H groups typically show lactam and pyrrole NH chemical shifts of ~10.5 and ~9 ppm [19, 22, 24]. This particular shielding of the pyrrole NH seems to be diagnostic of intramolecular hydrogen bonding. In Table 2 one finds a pyrrole chemical shift of 9.26 ppm for **1a**, which is very close to the 9.15 ppm value seen in *MBR-XIII* and related rubins [19]. The lactam signal in **1a** at 10.54 ppm and the deshielding of the CO_2H to 13.08 ppm provides added support to our conclusion that **1a** adopts an intramolecularly hydrogen-bonded conformation (Fig. 3B). Unfortunately, the lesser solubility of **1b** in $CDCl_3$ made it impossible to analyze for the expected *inter*molecular hydrogen bonding between dipyrrinones [26]. The greater solubility of **1a** in $CDCl_3$ allowed for $^1H\{^1H\}$-homonuclear N*O*E experiments, which showed the expected N*O*Es between the pyrrole and lactam NHs, and between the C(5, 15) olefinic hydrogens and the C(7, 13) methyls and C(3, 17) ethyls – all characteristic of the *syn-Z* configuration of the dipyrrinones. Only a faint N*O*E could be seen between the CO_2H and lactam NH, which might suggest somewhat weaker hydrogen bonding in **1a** than in bilirubin or *MBR-XIII*. In contrast, and as anticipated, ^1H NMR spectra of both **1a** and **1b** in $(CD_3)_2SO$ exhibit lactam NH and COOH chemical shifts characteristic of *MBR-XIII* (Table 2). The more deshielded pyrrole NH chemical shifts of **1a** and **1b** compared with the latter might be due to nearby effects of the acetylene groups. Many of the same N*O*Es seen above were also seen for **1a** and **1b** in $(CD_3)_2SO$ and are characteristic of the *syn-Z* configuration of the dipyrrinones.

Conformation Analysis from Molecular Dynamics

Independent rotations of the approximately planar, thermodynamically most stable *syn-Z*-dipyrrinones of **1a** or **1b** about the diacetylene unit (about ϕ_1 and ϕ_2 or ϕ_3, as illustrated for **1a** in Fig. 4) lead to an infinite number of conformations, including two high energy limiting cases (as determined by the Sybyl force field [27]) where the dipyrrinones lie coplanar: the *syn* and *anti*. Lying between these extremes is a conformation stabilized by intramolecular hydrogen bonding, given sufficient length of the alkanoic acid substituents at C(8) and C(12). In comparing **1a** and **1b**, molecular models show a better match for intramolecular hydrogen bonding with hexanoic acids (**1a**) than with propionic acids (**1b**): both CO_2H groups of **1a**

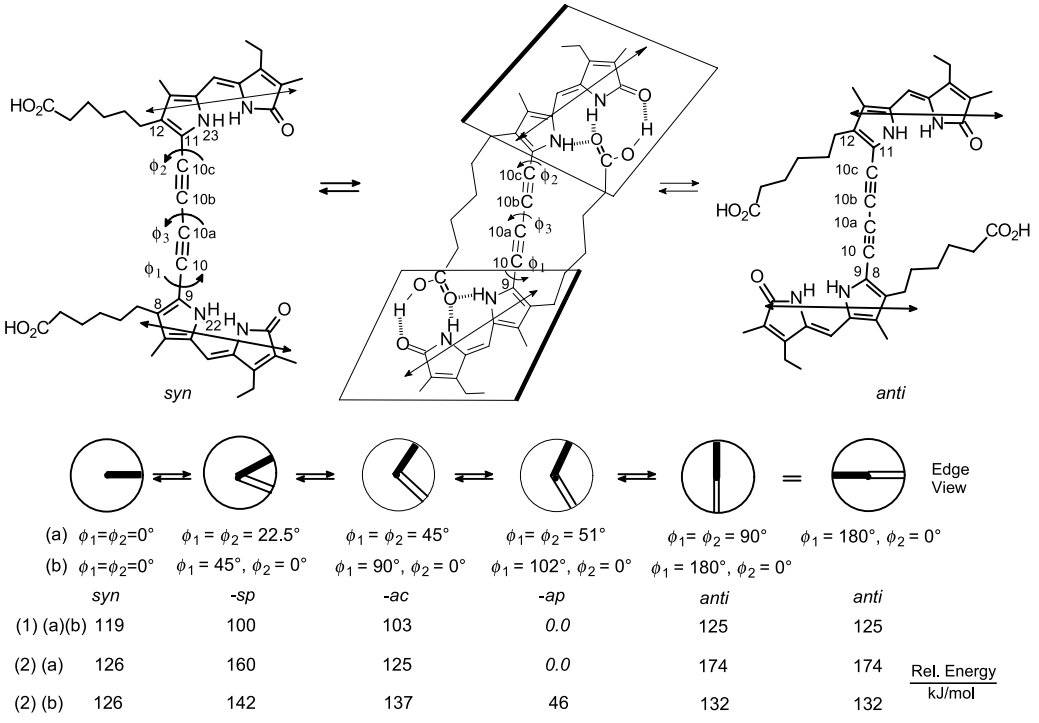

Fig. 4. Interconversion of conformations of **1a** by rotation about torsion angles $\phi_1 = $ N(22)–C(9)–C(10)–C(10a) and $\phi_2 = $ C(10b)–C(10c)–C(11)–N(23) as viewed edgewise from the C(2)–C(3)–C(5)–C(7) dipyrrinone backbone; the dark bar represents the long edge of the lower dipyrinnone; the open bar represents an edge view of the top dipyrinnone; in the eclipsed *syn* conformation, ϕ_1 and ϕ_2 are defined as 0°; the (+) rotations about ϕ_1 and ϕ_2 depicted interconvert the planar *syn*- and *anti*-conformations (an enantiomeric set of twisted conformations ($\phi_1 = \phi_2 \neq 0°, \neq 90°$) is created by (−) rotations); the relative energies associated with the designated conformers are shown below each; the $\phi_1 = \phi_2 = 60°$ global energy-minimum conformation is stablized by intramolecular hydrogen bonding; other combinations of rotations about ϕ_1 and ϕ_2, *e.g.*, $\phi_1 = 0°$, $\phi_2 = 180°$ also interconvert the *syn*- and *anti*-conformations; in rotations (a), the ϕ torsion angles are driven so that $\phi_1 = \phi_2$, in (b) ϕ_2 is held at 0° and ϕ_1 is driven from 0° to −180°; in (1), the C(9)–C≡C–C≡–C(11) fragment is constrained to be linear (*i.e.*, C(9)–C(10)–C(10a) = C(10)–C(10a)–C(10b) = C(10a)–C(10b)–C(10c) = C(10b)–C(10c)–C(11) = 180°) so that (a) and (b) track through identical conformers by rotation about the bond between the two acetylenes, and E (51°, 51°) = −69.9 kJ/mol); in (2) the constraint on these bond angles, and hence linearity, is lifted, which leads to some differing conformations between sets 1 and 2 as well as between 2(a) and 2(b), *e.g.*, $\phi_1 = \phi_2 = 90°$, and $\phi_1 = 180°$, $\phi_2 = 0°$; in 2(a) E (51°, 51°) = −73.6 kJ/mol; whereas in 2(b), E (102°, 0°) = −28 kJ/mol; the approximate locations of the dipyrrinone long wavelength electric dipole transition moments lie along the long axis of the chromophore, as indicated

are engaged in intramolecular hydrogen bonding to an opposing dipyrrinone; in **1b** neither CO_2H can become engaged. Conformational analysis by molecular dynamics calculations using Sybyl [27] gave an energy-minimum conformation of **1a** in which both hexanoic acid groups are engaged in intramolecular hydrogen bonding to an opposing dipyrrinone (Fig. 5), but for **1b**, neither propionic acid could do so. Lengthening both propionic acid chains to butyric or pentanoic was insufficient to allow both CO_2H groups to engage in intramolecular hydrogen

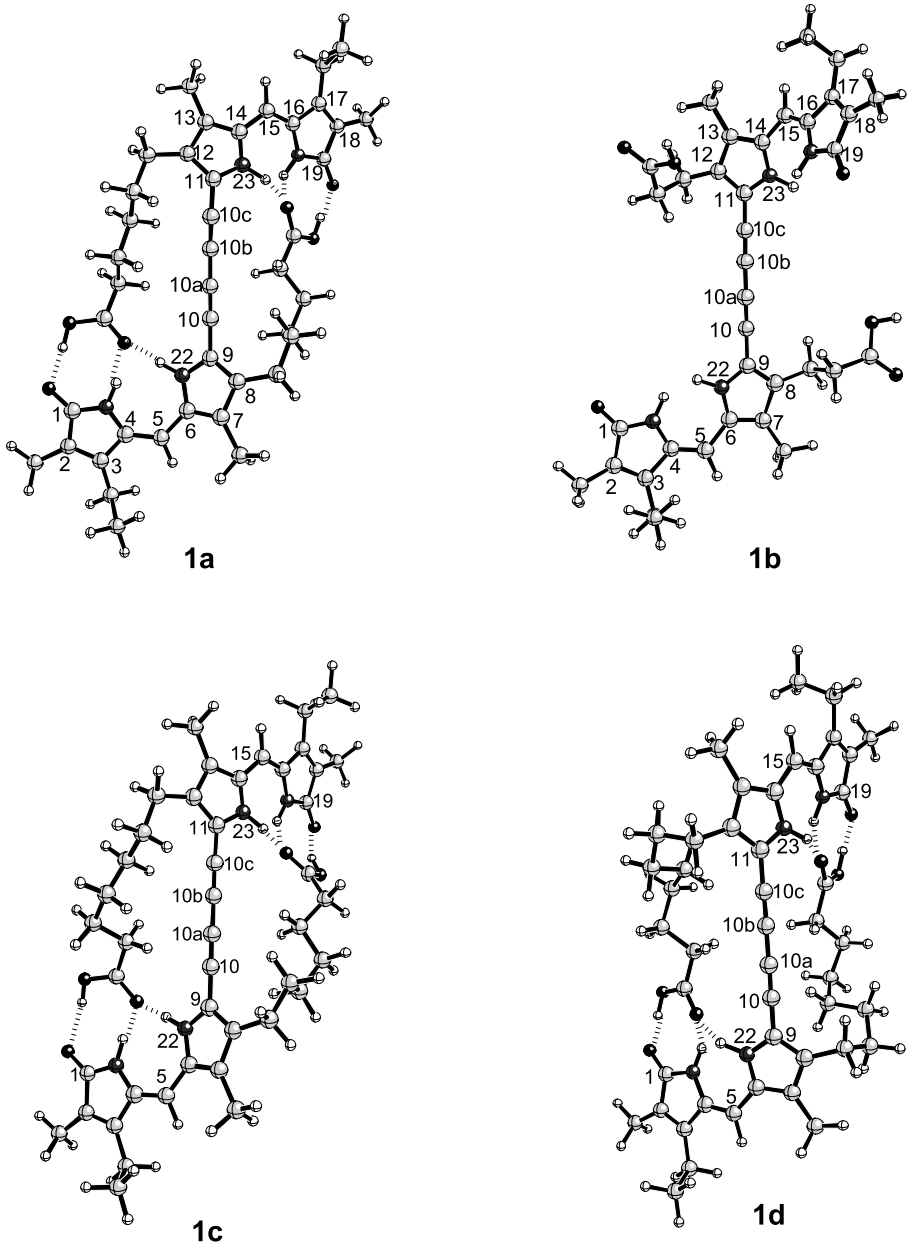

Fig. 5. Ball and Stick [27] representations of the minimum energy conformations of **1a** (bis-hexanoic acid), **1b** (bis-propionic acid), **1c** (bis-heptanoic acid), and **1d** (bis-octanoic acid) diacetylenic rubins as determined by molecular mechanics computations using the Sybyl forcefield; the relevant torsion angles (ϕ and ψ, in degrees) are: $\phi_1 = (22–9–10–10a)$, $\phi_2 = (10b–10c–11–23)$, $\psi_1 = (4–5–6–22)$, and $\psi_2 = (23–14–15–16)$; the bond angles (9–10–10a), (10–10a–10b), (10a–10b–10c), and (10b–10c–11) lie between 176 and 180°, with an average of 179°; the bond angles (22–9–10) and (10c–11–23) lie between 121 and 126°, with an average of 124°; in **1a**: $\phi_1 = \phi_2 = 51°$, $\psi_1 = -23°$, and $\psi_2 = 27°$; in **1b**: $\phi_1 = 71°$, $\phi_2 = 133°$, $\psi_1 = -35°$, and $\psi_2 = 35°$ (with the conformation lying in a broad well); in **1c**: $\phi_1 = 36°$, $\phi_2 = 130°$, $\psi_1 = 23°$, and $\psi_2 = 24°$; in **1d**, $\phi_1 = \phi_2 = 110°$, $\psi_1 = -15°$, and $\psi_2 = -20°$

bonding to the opposing dipyrrinones, however, chains longer than hexanoic, *e.g.*, heptanoic (**1c**) and octanoic (**1d**), allowed intramolecular hydrogen bonding to persist. In the energy-minimized structures of **1**, the extended planes of the dipyrrinones of each intersect along the $-(C{\equiv}C)_2-$ axis. In **1a** the extended planes intersect at an angle of 102°; in **1b** the intersection angle is ∼26°; in **1c** it is 166° ($\phi_1 = 36°$, $\phi_2 = 130°$); and in **1d** it is 40° ($\phi_1 = \phi_2 = 110°$). The latter two were not synthesized for this study, and their conformational data (Fig. 5) are included to show that the choice of alkanoic acid chain length can be used to fix varying interplanar angles between the two dipyrrinones and hence the conformation of the intramolecularly hydrogen-bonded diacetylene pigments.

In **1a** and **1b**, rotations about ϕ_1 and ϕ_2 (or ϕ_3) (illustrated for **1a** in (a) of Fig. 4), or for rotations about ϕ_1 while holding $\phi_2 = 0°$ (illustrated for **1a** in (b) of Fig. 4) interconvert planar *syn* and *anti* conformers, rotating them through twisted conformations. When the C(9)–C(10)–C(10a), C(10)–C(10a)–C(10b), C(10a)–C(10b)–C(10c), and C(10b)–C(10c)–C(11) bond angles are fixed at 180° ((1) of Fig. 4) in order to maintain strict linearity of the C(9)–C≡C–C≡C–C(11) fragment, rotation is effected about the C(10a)–C(10b) bond to generate sets of identical conformers in set 1(a)/1(b) of Fig. 4, *i.e.*, the conformer with $\phi_1 = \phi_2 = 45°$ is identical to that at $\phi_1 = 90°$, $\phi_2 = 0°$ (or $\phi_1 = 0°$, $\phi_2 = 90°$), and the conformer at $\phi_1 = \phi_2 = 90°$ is identical to that at $\phi_1 = 180°$, $\phi_2 = 0°$ (or $\phi_1 = 0°$, $\phi_2 = 180°$). For **1a**, the conformer at $\phi_1 = \phi_2 = 51°$ (identical to that at $\phi_1 = 102°$, $\phi_2 = 0°$) is found to lie at the global energy minimum because in this conformation each dipyrrinone and an opposing CO_2H group are fully engaged in intramolecular hydrogen bonding. In the other conformers, within the constraints imposed, the energy rises considerably as hydrogen bonds are broken by twisting away from $\phi_1 \sim \phi_2$ ∼51°. Thus, the ($\phi_1 = \phi_2 = 51°$) lies in a deep and narrow potential energy well.

When the constraint C(9)–C(10)–C(10a) = C(10)–C(10a)–C(10c) = C(10a)–C(10b)–C(10c) = C(10b)–C(10c)–C(11) = 180° is relaxed (set 2(a)/2(b) of Fig. 4), the $\phi_1 = \phi_2 = 51°$ conformer lies at a slightly lower global energy minimum (−73.6 kJ/mol in 2(a) *vs.* −69.9 kJ/mol in 1(a)/(b)) due to more effective intramolecular hydrogen bonding afforded by bending the two triple bonds with respect to each other, or by bending C(9) and C(11) out of strict linearity with the triple bonds in such a way that the C(9)–C(10)–C(10a) and C(10)–C(10a)–C(10b), C(10a)–C(10b)–C(10c) and C(10b)–C(10c)–C(11) bond angles are not exactly 180° and C(9)–C≡C–C≡C–C(11) is no longer linear (Table 3). When the restriction is lifted, the C(9)–C(10)–C(10a), C(10)–C(10a)–C(10b), and C(10b)–C(10c)–C(11) bond angles bend between 0° and 9° out of linearity and the dipyrrinone torsion angles (ψ_1 and ψ_2) twist more or less severely in set (2) than in set (1) of Table 3. One consequence of lifting strict linearity of diacetylene axis in set (2) is that the (a) and (b) conformations are not necessarily identical, *e.g.*, ($\phi_1 = \phi_2 = 90°$) and ($\phi_1 = \phi_2 = 45°$) no longer correspond exactly to ($\phi_1 = 180°$, $\phi_2 = 0°$) and ($\phi_1 = 90°$, $\phi_2 = 0°$), respectively (Table 3) due to a differing ability to participate in intramolecular hydrogen bonding. A second consequence is that the C(9) and C(11) atoms do not necessarily bend out of linearity in the same plane, *e.g.*, in conformers ($\phi_1 = \phi_2 = 51°$) and ($\phi_1 = 102°$, $\phi_2 = 0°$) the C(10)–C(10a)–C(10b) and C(10c) torsion angles (ϕ_3) are −3.7° and 93.4°, respectively, and for ($\phi_1 = \phi_2 = 90°$) and ($\phi_1 = 180°$, $\phi_2 = 0°$) the torsion angles are −12.1° and −8.8°,

Table 3. Conformations and relative energies of **1a** determined by bond angles and torsion angles ϕ and ψ[a]

Data set[b]	$\phi_1/^\circ$	$\phi_2/^\circ$	$\phi_3/^\circ$	Bond angles[b]/°				$\psi_1/^\circ$	$\psi_2/^\circ$	ΔE[c]
	(22–9–10–10a)	(10b–10c–11–23)	(10–10a–10b–10c)	(9–10–10a)	(10–10a–10b)	(10a–10b–10c)	(10b–10c–11)	(4–5–6–22)	(23–14–15–16)	kJ/mol
(1a, b)	0	0	0	180	180	180	180	−22	26	119
(1a, b)	22.5	22.5	0	180	180	180	180	−36	34	100
(1a, b)	45	45	0	180	180	180	180	−35	35	103
(1a, b)	51	51	0	180	180	180	180	−20	26	0
(1a, b)	90	90	0	180	180	180	180	−34	36	125
(2a, b)	0	0	4.6	179	179	177	177	−22	26	126
(2a)	22.5	22.5	65.3	180	176	174	178	30	−52	160
(2b)	45	0	4.7	179	179	177	177	26	−22	142
(2a)	45	45	145.2	180	179	179	178	30	−34	126
(2b)	90	0	69.6	179	179	179	178	43	−43	138
(2a)	51	51	−3.7	179	178	177	176	26.5	−23	0
(2b)	102	0	93.4	175	178	173	174	21	−14	46
(2a)	90	90	−12.1	171	176	175	178	43	−23	176
(2b)	180	0	−8.8	178	179	179	178	31	−36	134

[a] Refer to Fig. 4 for numbering and reference systems used; [b] data set (1) refers to conformations in which 180° linearity is maintained by forcing bond angles 9–10–10a, 10–10a–10b, 10a–10b–10c, and 10b–10c–11 at 180°; in data set (2) this constraint is lifted; in both (1)(a) and (b) the computed bond angles (22–9–10) and (10c–11–23) lie between 121° and 126°; in (2) they lie between 119° and 128°; [c] ΔE of (1) is relative to the $\phi_1 = \phi_2 = -51^\circ$ energy minimum of −69.9 kJ/mol; ΔE of (2)(a) is relative to the $\phi_1 = \phi_2 = -51^\circ$ energy minimum of −73.6 kJ/mol; thus, all values of (1) are ∼4 kJ/mol higher energy than the corresponding (ϕ_1, ϕ_2) conformers of (2a); ΔE of (2)(b) is relative to the $\phi_1 = \phi_2 = 51^\circ$ energy minimum of −31.8 kJ/mol

respectively (Table 3). Thus, when C(9) and C(11) do not bend out of linearity in the same plane, the ($\phi_1 = 102°$, $\phi_2 = 0°$) and ($\phi_1 = \phi_2 = 51°$) conformers are clearly not identical. The distortion from linearity in the ($\phi_1 = 102°$, $\phi_2 = 0°$) conformer is strikingly large compared to the rather minimal distortion in the ($\phi_1 = \phi_2 = 51°$) global energy minimum conformer. Nevertheless, these two energy minimum conformations retain full intramolecular hydrogen bonding. As the ϕ_1 and ϕ_2 angles are rotated away from those found in the energy minima, intramolecular hydrogen bonds are severed, with a concomitant steep rise in energy. Here, as in set 1(a)/1(b) of Fig. 4, the energy-minima lie in a steep, narrow well. Most likely with longer alkanoic acid chains, *e.g.*, heptanoic (**1c**) or octanoic (**1d**) (Fig. 5), intramolecular hydrogen bonding would be retained over a wider range of conformations.

Conformation from UV-Visible and Induced Circular Dichroism Spectra

Additional evidence on the conformation of **1a** and **1b** comes from solvent-dependent UV-visible spectra. Compared with their parent rubin (*MBR-XIII*, with broad absorption near 430 nm and a shoulder near 395 nm in most solvents), diacetylene rubins **1a** and **1b** showed (Table 4) a broad band centered near 460 nm, a shorter wavelength band near 410 nm and a prominent (or dominant) longer wavelength (∼510 nm) band, which thus accounts for the red color of these pigments. Over a wide range of solvents of varying polarity and hydrogen bonding ability (benzene, chloroform, acetone, methanol, acetonitrile, and dimethylsulfoxide), the UV-Vis long wavelength absorbance, *i.e.*, λ_{max} of **1a** and **1b** show greater solvent-dependence than of *MBR-XIII* (Table 4), with 10–15 nm hypsochromic shifts from benzene, $CHCl_3$, and $(CH_3)_2SO$ to $(CH_3)CO$, CH_3OH, and CH_3CN. The absorptivity of this band is greater in **1a** than **1b**. Smaller hypsochromic shifts attend the 408 nm band of **1a** and **1b**, but the ∼460 nm band of **1a** remains relatively invariant in λ_{max} (except for $CHCl_3$) and in intensity.

In the UV-Vis of *MBR-XIII*, the long wavelength absorption near 430 nm originates from exciton coupling [9, 28], from electric dipole-electric dipole transition moment interaction of the two dipyrrinone chromophores. The dipyrrinone

Table 4. Solvent-dependence of the UV-visible spectral data of diacetylenic rubins **1a** and **1b** with mesobilirubin-XIIIα (*MBR-XIII*); at 22°C in concentrations $\sim 1.4 \times 10^{-5}\, M$

Compound	$\varepsilon^{max}/dm^3 \cdot mol^{-1} \cdot cm^{-1}$ (λ^{max}/nm)					
	Benzene	$CHCl_3$	$(CH_3)_2CO$	CH_3OH	CH_3CN	$(CH_3)_2SO$
1a	42600 (516)[a]	62400 (520)	41300 (506)[a]	46400 (507)[a]	45800 (509)	35700 (515)[a]
	53400 (465)	60400 (490)[a]	56300 (457)	60600 (461)	56200 (461)[a]	57800 (460)
	34000 (408)[a]	24200 (410)[a]	34500 (401)[a]	41200 (401)[a]	33000 (401)[a]	41200 (409)[a]
1b	33700 (513)[a]	26000 (513)[a]	27200 (503)[a]	24800 (502)[a]	25000 (507)[a]	21000 (512)[a]
	46300 (465)	42000 (462)	46600 (453)	46900 (451)	48500 (456)	42900 (456)
	26900 (406)[a]	30600 (407)[a]	31500 (401)[a]	32400 (398)[a]	34100 (401)[a]	41000 (406)[a]
MBR-XIII	49900 (439)	50300 (431)	49700 (427)	50600 (425)	49000 (425)	52500 (428)

[a] Shoulders (or) inflections were determined by first and second derivative spectra

chromosphores of this study typically exhibit UV-Vis $\lambda_{max} \sim 400–420$ nm for their long wavelength absorption band, with the electric transition dipole moment lying along the long axis of the chromophore [28]. The origin of the UV-Vis bands of **1a** and **1b** is not entirely clear. The ~510 nm band is considerably red-shifted from the usual dipyrrinone λ_{max} (400–420 nm). Unless the diacetylene group is exerting a large shift on the dipyrrinone chromophore, the ~510 nm band might be viewed as originating in conjugation rather than from exciton coupling [30], leaving the ~460 and ~405 nm bands as the two components of an exciton interaction, both flanking the dipyrrinone 400–420 nm λ_{max}. Alternatively, one might view the ~510 and ~460 nm bands as originating from exciton coupling between two C(9)–C≡C– dipyrrinones, whose UV-Vis characteristics remain unknown. In either case, the UV-Vis data of both **1a** and **1b** suggest that oblique orientations of the dipyrrinone electric dipole transition moments are maintained in the solvents studied.

In exciton coupling theory, the relative orientation of the relevant electric dipole transition moments can be important to stereochemical analysis of bis-dipyrrinones [9, 28]. When linked to the ends of a diacetylene, dipyrrinones may rotate into a large number of relative orientations, of which two limiting planar conformations, *syn* and *anti*, become apparent. In the (planar) *anti* conformer (Fig. 4), the dipyrrinone long wavelength electric dipole transition moments associated with the ~410 nm UV-Vis absorption of the dipyrrinone chromophore lie in-line, which would suggest a red-shifted exciton band [30]. In the *syn*, they lie in the same plane and nearly parallel, which would yield a blue-shifted exciton band. The planar conformations are achiral, and the relevant dipyrrinone electric dipole transition moments lie in a common plane. However, there are many other conformations, all chiral, originating by rotating the dipyrrinones about the –C≡C–C≡C– axis. In such conformations, the planes encompassing each dipyrrinone are not coincident and thus the dipyrrinone electric dipole transition moments have a chiral, helical (''oblique'' [30], Fig. 6) relative orientation. For the twisted conformers, exciton coupling theory thus predicts intensity from both exciton transitions and hence a broadened UV-Vis absorption curve, or one with the two exciton bands separated to some extent. This is seen in the UV-Vis spectra of both **1a** and **1b**.

Unlike bilirubin, the diacetylenic rubins of this work cannot be folded into ridge-tile shapes such as Fig. 1C; however, intramolecular hydrogen bonding (Fig. 6) can preserve a linear, rotated conformation. As the two dipyrrinones approach the coplanarity of the *anti* conformation (Fig. 4), the orientation of the relevant electric transition dipoles tends toward the ''in-line'' orientation, as in the intramolecularly hydrogen-bonded structures. In such conformations, the long wavelength component of the exciton couplet is expected to dominate – as may be noted in the ~460/~405 nm bands of the UV-Vis spectra of **1a** and **1b**. In $CHCl_3$ with added quinine [28], **1b** shows what one might see as intense a *positive* exciton chirality CD [31] with a positive *Cotton* effect near 460 nm and a negative *Cotton* effect near 404 nm, with $|\Delta\varepsilon \geq 100\,dm^3 \cdot mol^{-1} \cdot cm^{-1}$ (Spectrum II, Fig. 7). This is followed by a moderately strong ($\Delta\varepsilon \sim -25\,dm^3 \cdot mol^{-1} \cdot cm^{-1}$) near 520 nm. The data are consistent with an exciton couplet for the 460/405 nm UV-Vis bands, and suggest that twisted a conformation dominates the CD spectrum of

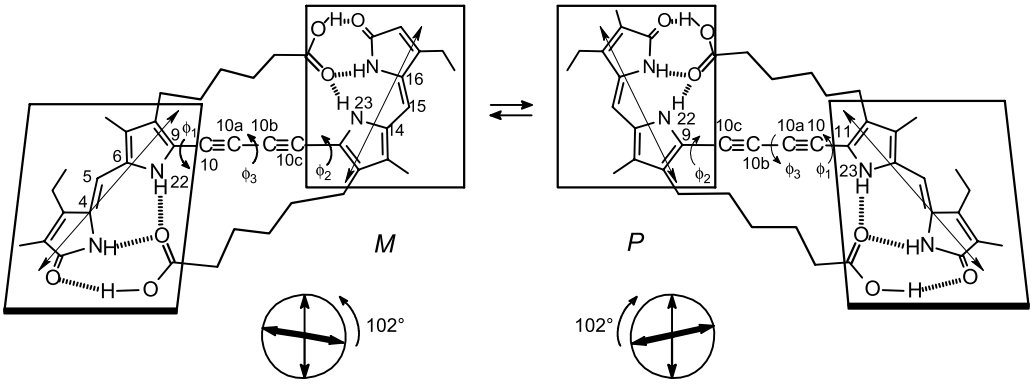

Fig. 6. Twisted, intramolecularly hydrogen-bonded enantiomeric (*M* and *P*) conformations of the diacetylenic rubin with hexanoic acid chains (**1a**); interconversion is accomplished by rotating about ϕ_1 and ϕ_2; in *M* and *P*, each dipyrrinone chromophore is approximately planar, with torsion angles C(4)–C(5)–C(6)–N(22) and N(23)–C(14)–C(15)–C(16) ∼23°, and the angle of intersection of the two planes (dihedral angle, θ) is ∼102° for $\phi_1 \sim \phi_2$ ∼51°; the double-headed arrows represent the approximate direction and intensity of the dipyrrinone long wavelength electric transition dipole moments; the relative orientations or helicities (*M*, minus; *P*, plus) of the vectors are shown (inset) for each enantiomer; for these conformations, the *M* dipole helicity correlates with the *M* molecular chirality and the *P* helicity with the *P* molecular chirality

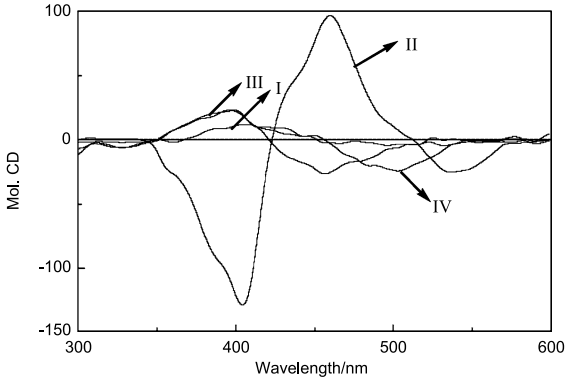

Fig. 7. Comparison of the circular dichroism (CD) and UV-visible spectroscopic data of **1a** and **1b** in $CHCl_3$ solutions containing quinine (I and II, pigment conc. $\sim 1.4\times10^{-5}\,M$; quinine conc. $\sim 4.2\times10^{-3}\,M$; pigment:quinine molar ratio = ∼1:300) and in *HSA* $pH = 7.4$ tris buffer (III and IV, pigment conc. $\sim 1.4\times10^{-5}\,M$, *HSA* conc. $2.8\times10^{-5}\,M$); spectrum I: **1a**, $CHCl_3$: $\Delta\varepsilon_{403}^{max} = +18$, $\Delta\varepsilon_{422} = 0$, $\Delta\varepsilon_{457}^{max} = -26$; UV-Vis: $\varepsilon_{483}^{max} = 53200$; spectrum II: **1b**, $CHCl_3$: $\Delta\varepsilon_{404}^{max} = -129$, $\Delta\varepsilon_{423} = 0$, $\Delta\varepsilon_{460}^{max} = +96$; UV-Vis: $\varepsilon_{465}^{max} = 51700$; spectrum III: **1a**, *HSA*: $\Delta\varepsilon_{398}^{max} = +22$, $\Delta\varepsilon_{451} = 0$, $\Delta\varepsilon_{533}^{max} = -5.2$; UV-Vis: $\varepsilon_{494}^{max} = 50800$; spectrum IV: **lb**, *HSA*: $\Delta\varepsilon_{398}^{max} = +23$, $\Delta\varepsilon_{456} = 0$, $\Delta\varepsilon_{504}^{max} = -25$; UV-Vis: $\varepsilon_{466}^{max} = 38200$ (units of ε and $\Delta\varepsilon$ are $dm^3 \cdot mol^{-1} \cdot cm^{-1}$, units of λ are nm)

1b with a positive helical orientation of the dipyrrinone electric dipole transition moments, according to exciton coupling theory [31] and consistent with the *+sc* conformation.

In contrast, **1a** exhibits a significantly weaker *negative* exciton chirality CD (Fig. 7, Spectrum I), with a long wavelength negative *Cotton* effect

($\Delta\varepsilon = -26\,\mathrm{dm}^3 \cdot \mathrm{mol}^{-1} \cdot \mathrm{cm}^{-1}$) near 460 nm and a shorter wavelength negative *Cotton* effect ($\Delta\varepsilon = -18\,\mathrm{dm}^3 \cdot \mathrm{mol}^{-1} \cdot \mathrm{cm}^{-1}$) near 400 nm. The data are again consistent with an exciton couplet for the 460/405 nm bands and suggest dominant $-ap$ or $-ac$ conformations reflecting probably the near planarity of the two dipyrrinones. Apparently, the pigment (**1b**) that is not intramolecularly hydrogen-bonded coordinates strongly to the quinine in $CHCl_3$ adopting a chiral conformation dictated by the alkaloid. In contrast when intramolecularly hydrogen bonding also comes into play, a different chiral conformation is dictated.

In $pH = 7.4$ aqueous buffered human serum albumin (*HSA*) both **1a** and **1b** exhibit rather weak negative chirality bisignate CD curves with a broad negative ($\Delta\varepsilon = -5$ to $-25\,\mathrm{dm}^3 \cdot \mathrm{mol}^{-1} \cdot \mathrm{cm}^{-1}$) *Cotton* effect near ~505–530 nm and a positive *Cotton* effect ($\Delta\varepsilon = +23\,\mathrm{dm}^3 \cdot \mathrm{mol}^{-1} \cdot \mathrm{cm}^{-1}$) near 400 nm. Complexation of an $+sc$ or $+ac$ twisted conformation of **1** is apparently preferred. In contrast to the dissimilar CD spectra of **1a** and **1b** in $CHCl_3$ with quinine, the similarity of the bisignate *Cotton* effects of **1a** and **1b** is an indication that neither intramolecular hydrogen bonding (in **1a**) nor its absence (in **1b**) is a contributing factor in conformation and chirality of the pigments complexed to *HSA*. In this connection, it may be noted that *MBR-XIII* exhibits a well-defined positive chirality exciton coupling bisignate CD ($\Delta\varepsilon_{436}^{\max} = +37$, $\Delta\varepsilon_{388}^{\max} = -42\,\mathrm{dm}^3 \cdot \mathrm{mol}^{-1} \cdot \mathrm{cm}^{-1}$) in $pH =$ 7.4 aqueous buffered *HSA* [32].

Experimental

Nuclear magnetic resonance (NMR) spectra were obtained in $CDCl_3$ solvent on a GE QE-300 spectrometer operating at 300 MHz (unless otherwise indicated), or on a Varian Unity Plus 500 MHz spectrometer. HMQC, HMBC, and N*O*E NMRs were obtained at 500 MHz spectrometer. Chemical shifts were reported in δ ppm referenced to the residual $CHCl_3$ ^1H signal at 7.26 ppm and ^{13}C at 77.23 ppm. Infrared spectra were recorded on a Perkin-Elmer model 1610-FT IR instrument. Ultraviolet-visible spectra were recorded on a Perkin-Elmer λ-12 spectrophotometer, *GC-MS* analyses were carried out on a Hewlett-Packard *GC-MS* Model 5890A ion selective detector equipped with a DB-l (100% dimethylpolysiloxane) column. Melting points were taken on a Mel-Temp capillary apparatus and are uncorrected. Combustion analyses for carbon, hydrogen, and nitrogen were carried out by Desert Analytics, Tucson, AZ, and gave results within $\pm 0.4\%$ of the theoretical values. High resolution mass spectra were obtained from the Nebraska Center for Mass Spectrometry (Univ. Nebraska-Lincoln). Analytical thin layer chromatography (TLC) was carried out on J.T. Baker silica gel IB-F plates (125 μm layers). Flash column chromatography was carried out using silica gel, 60–200 mesh (M. Woelm). Radial chromatography was carried out on Merck preparative layer grade silica gel PF_{254} with $CaSO_4$ binder using a Chromatotron (Harrison Research, Inc., Palo Alto, CA) with 1, 2, or 4 mm thick rotors. HPLC analyses were carried out on a Perkin-Elmer Series 4 high performance liquid chromatograph with a LC-95 UV-Vis spectrophotometric detector (410 nm). The column was a Beckman-Altex ultrasphere-IP 5 μm C-18 ODS column (25 × 0.46 cm) fitted with a similary-packed precolumn (4.5 × 0.46 cm). The flow rate was 0.75–1.0 cm^3/min; the elution solvent was 0.1 *M* di-*n*-octylamine acetate in 5% aqueous CH_3OH, the column temperature was ~34°C. (Trimethylsilyl)acetylene was from GFS Chemicals. Ceric ammonium nitrate (*CAN*) was from Alfa Aesar. Dichlorobis(triphenylphosphine)palladium(II) and tetrakis(triphenyl-phosphine)palladium(0) were from Aldrich. Commercial reagents were used as received from Aldrich or Acros; HPLC grade CH_3OH was from Fisher; human serum albumin (defatted) was obtained from Sigma. Spectroscopic data were obtained in spectral grade solvents from Fisher and Acros. Deuterated chloroform and dimethylsulfoxide were from Cambridge Isotope Laboratories. Pyrroles **5b**–**11b** were available from previous work [33].

UV and CD Measurements

A stock solution of $\sim 7.0 \times 10^{-4}$ *M* of **1a** and **1b** was prepared by dissolving an appropriate amount of the desired pigment in 2 cm^3 of *DMSO*. Next, a 0.1 cm^3 aliquot of the stock solution was diluted to 5 cm^3 (volumetric flask) the specified organic solvent for UV-Vis studies (Table 4) or, for CD studies involving human serum albumin (*HSA*), with an *HSA* solution ($\sim 2.8 \times 10^{-5}$ *M* in $pH = 7.4$ Tris buffer). The final concentration of the solution was $\sim 1.4 \times 10^{-5}$ *M* in pigment. Up to four 5 cm^3 solutions of each pigment were prepared, as needed, in 5 cm^3 volumetric flasks. For CD studies in $CHCl_3$, solutions were prepared directly in $CHCl_3$ containing a 300:1 molar ratio of quinine:pigment to give final concentrations of $\sim 1.4 \times 10^{-5}$ *M* in pigment.

Potassium Ethyl Pimelate (**14**, $C_9H_{15}O_4K$)

To a solution of 6.47 g of KOH in 100 cm^3 of absolute ethanol was added slowly 25 g (115.7 mmol) of diethyl pimelate (**15**) in 30 min. The reaction mixture was stirred at 50°C for 16 h during which some solid was precipitated. The solvent was evaporated on a roto-vap and the residue was washed with cold hexane and filtered to afford a white solid. Yield 21 g (80%); mp 280–282°C (Ref. [34] 273–275°C); ^{1}H NMR (*DMSO*-d_6): $\delta = 1.12$ (t, $J = 7.2$ Hz, 3H), 1.33 (m, 2H), 1.43 (m, 2H), 1.73 (t, $J = 7.2$ Hz, 2H), 2.19 (t, $J = 7.2$ Hz, 2H), 3.98 (q, $J = 7.2$ Hz, 2H) ppm.

6-Carbethoxypentanoyl Chloride (**13**, $C_9H_{15}O_3Cl$)

To a suspension of 21 g (93 mmol) of potassium ethyl pimelate (**14**) in 70 cm^3 of dry benzene was added slowly over 40 min a solution of 9 cm^3 of oxalyl chloride in 70 cm^3 of dry benzene at 0°C. The mixture was stirred at the same temperature for another hour until bubbling had ceased; then the solvent and unreacted oxalyl chloride were removed under vacuum. The gelatinous residue was sufficiently pure for the next step. ^{1}H NMR: $\delta = 1.15$ (t, $J = 7.1$ Hz, 3H), 1.24 (m, 2H), 1.46 (m, 4H), 2.14 (t, $J = 7.2$ Hz, 2H), 2.22 (t, $J = 7.2$ Hz, 2H), 3.98 (q, $J = 7.1$ Hz, 2H) ppm.

Ethyl 5-Carboxy-2,3-dimethyl-1H-pyrrole-4-hexanoate (**11a**, $C_{17}H_{27}NO_4$)

To a suspension of anhydrous $ZnCl_2$ in 90 cm^3 of dry CH_2Cl_2 was added **13** (above) at 0°C, then a mixture of 14.1 g of 2-(trimethylsilyloxy)-2-butenes was added slowly. The mixture was stirred at 0°C for 3 h and became yellow. The yellow solution was poured into 300 cm^3 of water and extracted with 3×200 cm^3 of CH_2Cl_2 until the extract became colorless. The combined organic layers were washed with 3×100 cm^3 of saturated $NaHCO_3$ solution, water, and saturated NaCl solution. After drying over anhydrous Na_2SO_4, the residue, after evaporation of the solvent, gave the expected ethyl 7,9-dioxo-8-methyldecanoate (**12a**). It was sufficiently pure (analyzed by GC-MS) for the next step. MS: $m/z = 242$ [$M^{+\bullet}$], 197, 171, 155, 125, 99, 97, 55; ^{1}H NMR: $\delta = 1.25$ (t, $J = 7.2$ Hz, 3H), 1.32 (d, $J = 7.5$ Hz, 3H), 1.37 (m, 2H), 2.17 (s, 3H), 2.30 (t, $J = 7.2$ Hz, 2H), 2.32 (m, 4H), 2.36 (t, $J = 7.2$ Hz, 2H), 3.67 (q, $J = 7.2$ Hz, 1H), 4.13 (q, $J = 7.2$ Hz, 2H) ppm.

Ethyl 7,9-dioxo-8-methyldecanoate (**12a**) above was added to 50 cm^3 of HO*Ac* and heated slowly to 80°C, then 11 g of anhydrous NaO*Ac* and 8.7 g of Zn dust were added in three portions. The mixture was heated to 90°C, followed by dropwise addition of 7.67 g of diethyl oximinomalonate in a solution of 13 cm^3 of HO*Ac* and 4 cm^3 of H_2O. The mixture was heated at reflux for 3 h and then poured into 1000 cm^3 of ice and left to stand for 1 h at room temperature. The solution was extracted with 3×300 cm^3 of CH_2Cl_2, and the combined extracts were washed with saturated 3×100 cm^3 of $NaHCO_3$ solution, water, and saturated NaCl solution. After drying over anhydrous Na_2SO_4, and evaporation of the solvent, a pale yellow oil was obtained. An analytical sample could be prepared by recrystallization from ethanol–H_2O as a white solid. Overall yield 6 g (16.8%); mp 54–56°C; IR (NaCl, film): $\bar{\nu} = 3446$, 3054, 2984, 1726, 1667, 1429, 1265, 1172, 1028, 896, 738, 705 cm^{-1}; ^{1}H NMR: $\delta = 1.22$

(t, $J = 7.2$ Hz, 3H), 1.33 (t, $J = 7.2$ Hz, 3H), 1.40 (m, 2H), 1.50 (m, 2H), 1.65 (m, 2H), 1.91 (s, 3H), 2.18 (s, 3H), 2.29 (t, $J = 7.5$ Hz, 2H), 2.69 (t, $J = 7.5$ Hz, 2H), 4.12 (q, $J = 7.2$ Hz, 2H), 4.29 (q, $J = 7.2$ Hz, 2H), 8.54 (brs, 1H) ppm; ^{13}C NMR: $\delta = 8.7$, 11.3, 14.2, 14.5, 24.9, 25.0, 29.1, 30.4, 34.3, 59.4, 60.0, 116.2, 116.5, 129.6, 132.2, 161.5, 173.8 ppm; GC-MS: m/z (%) = 309 [$M^{+\bullet}$], 364, 236, 180 (100), 134, 108, 79.

Ethyl 5-Carbethoxy-2-formyl-3-methyl-1H-pyrrole-4-hexanoate (**10a**, $C_{17}H_{25}NO_5$)

To a solution of 4.2 g (13.6 mmol) of pyrrole **11a** in 140 cm^3 of *THF*, 40 cm^3 of HO*Ac*, and 140 cm^3 of H_2O was added 32 g (4 mol equiv) of ceric ammonium nitrate (*CAN*) in one portion at 0°C. The mixture was stirred at 0° for 1.5 h and then poured into 500 cm^3 of H_2O. The mixture was extracted with 3×300 cm^3 of $CHCl_3$, and then washed with saturated $NaHCO_3$ solution and saturated NaCl solution and H_2O. The organic solution was dried over anhydrous Na_2SO_4 and passed through a short column of silica gel using $CHCl_3$ as eluent. The eluent was evaporated to afford pyrrole aldehyde **10a** as a colorless oil. An analytical sample could be prepared by crystallization from hexane-$CHCl_3$ to afford white crystals. Yield 3.3 g (75%); mp 36–38°C; IR (NaCl, film): $\bar{\nu} = 3421$, 3055, 2987, 2306, 1720, 1655, 1461, 1422, 1265, 896, 739 cm^{-1}; ^{1}H NMR: $\delta = 1.24$ (t, $J = 7.05$ Hz, 3H), 1.37 (t, $J = 7.05$ Hz, 2H), 1.49 (m, 2H), 1.65 (m, 4H), 2.26 (m, 2H), 2.29 (s, 3H), 2.72 (t, $J = 7.5$ Hz, 2H), 4.12 (q, $J = 7.5$ Hz, 2H), 4.35 (q, $J = 7.5$ Hz, 2H), 9.42 (brs, 1H), 9.76 (s, 1H) ppm; ^{13}C NMR: $\delta = 8.4$, 14.2, 14.3, 24.0, 24.8, 29.0, 30.1, 34.2, 60.1, 60.8, 124.1, 129.6, 130.0, 131.8, 160.6, 173.6, 179.0 ppm; GC-MS: m/z (%) = 324 [$M^{+\bullet}$], 278, 250, 184, 166, 148 (100), 92, 65.

5-Carboxy-2-formyl-3-methyl-1H-pyrrole-4-hexanoic acid (**9a**, $C_{13}H_{17}NO_5$)

To a solution of 2.7 g (8.36 mmol) of pyrrole **10a** in 90 cm^3 of *THF*:H_2O (5:1 by vol) was added 1.41 g (33.4 mmol, 4 mol equiv) of $LiOH \cdot H_2O$. The mixture was stirred at 70°C for 4 h under N_2 and then cooled to room temperature. The red aqueous layer was washed with 3×80 cm^3 of ether and acidified carefully at 0°C with a saturated aqueous $NaHSO_4$ solution until the *pH* was about 3, the mixture was stirred at 0°C for an additional 30 min, until all the oil solidified. The solid was filtered and washed with a small amount of cold water to afford pyrrole diacid. Yield 1.7 g (76%); mp 138–140°C; IR (KBr, film): $\bar{\nu} = 3464$, 3211, 2934, 2862, 2589, 1702, 1604, 1553, 1467, 1380, 1249, 84, 768, 675 cm^{-1}; ^{1}H NMR (*DMSO*-d_6): $\delta = 1.$ 24 (m, 2H), 1.37 (m, 2H), 1.46 (m, 2H), 2.12 (t, $J = 6.9$ Hz, 2H), 2.18 (s, 3H), 2.61 (t, $J = 7.2$ Hz, 2H), 9.72 (s, 1H), 12.21 (brs, 1H), 12.31 (brs, 1H) ppm; ^{13}C NMR (*DMSO*-d_6): $\delta = 9.5$, 23.7, 24.7, 28.8, 30.3, 34.0, 124.6, 126.5, 130.8, 131.2, 162.3, 174.8, 182.2 ppm.

Methyl 2-Formyl-5-iodo-3-methyl-1H-pyrrole-4-hexanoate (**7a**, $C_{13}H_{18}INO_3$)

To a solution of 3.98 g of KI and 3.05 g of iodine in 24 cm^3 of H_2O was added slowly a solution of 1.6 g (6.0 mmol) of pyrrole diacid **9a** and 1.5 g of $KHCO_3$ in 24 cm^3 of H_2O. The reaction mixture was stirred at 65°C for an hour and then heated to reflux for 2 h while carbon dioxide evolved and the color gradually lightened. The reaction mixture was poured into 200 cm^3 of H_2O and extracted with dichloromethane until the organic layer was colorless. The extraction was dried over anhydrous Na_2SO_4 and evaporated to dryness. The residue, which was comprised mainly of 5-iodo-2-formyl-3-methyl-1*H*-pyrrole-4-hexanoic acid (**8a**), was used directly in the next step. To a 100 cm^3 flask were added a solution of 15 g of KOH in 15 cm^3 of H_2O and 120 cm^3 of ether. The solution was cooled to 0°C and 0.55 g of *N*-methyl-*N*-nitrosourea were added and stirred slowly for 10 min. The yellow ether layer was decanted and poured into a solution of **8a** in 100 cm^3 of methanol in two portions over 5 min. The reaction mixture was stirred for another 10 min until N_2 no longer evolved. Then 1 cm^3 of glacial acetic acid was added to destroy any excess diazomethane. The mixture was poured into 200 cm^3 of H_2O and

extracted with $3\times100\,cm^3$ of CH_2Cl_2, the combined organic layers were washed with $2\times100\,cm^3$ of H_2O, $2\times100\,cm^3$ of saturated $NaHCO_3$ solution, $2\times100\,cm^3$ of brine, and dried over anhydrous Na_2SO_4. After evaporation of the solvent, the residue was recrystallized from chloroform-hexane to give pure product **7a**. Yield 0.5 g (1.38 mmol, 23%); mp 86–87°C; IR (NaCl, film): $\bar{\nu} = 3420$, 3224, 3054, 2937, 1731, 1632, 1415, 1364, 1165, 896, 822, 739 cm^{-1}; ^1H NMR: $\delta = 1.37$ (t, $J = 7.7$ Hz, 2H), 1.46 (m, $J = 7.9$ Hz, 2H), 1.64 (m, 2H), 2.30 (s, 3H), 2.31 (t, $J = 7.2$ Hz, 2H), 2.36 (t, $J = 7.5$ Hz, 2H), 3.66 (s, 3H), 9.39 (s, 1H), 9.67 (brs, 1H) ppm; ^{13}C NMR: $\delta = 9.0$, 24.7, 26.0, 28.7, 29.6, 33.9, 51.4, 81.0, 130.1, 130.8, 133.9, 174.1, 176.0 ppm; GC-MS: m/z (%) = 363 [$M^{+\bullet}$], 304, 248 (100), 208, 176, 134, 122, 65.

Methyl 2-Formyl-3-methyl-5-[(trimethylsilyl)ethynyl]-1H-pyrrole-4-hexanoate (**6a**, $C_{18}H_{27}NO_3Si$)

To a solution of 290 mg (0.8 mmol) of methyl 2-formyl-5-iodo-3-methyl-1*H*-pyrrole-4-hexanoate (**7a**) in 8 cm^3 of diethylamine were added under N_2 0.12 g (1.2 mmol, 0.172 cm^3) of trimethylsilylacetylene, 10 mg (0.014 mmol) of dichlorobis(triphenyphosphine)palladium(II), and 5.2 mg (0.028 mmol) copper(I) iodide. The homogeneous mixture was stirred at 50°C for 1 h, during which the color became yellow, and a brown oil separated. After evaporation of the solvent in vacuum, the residue was subjected to chromatography on a short column of silica gel using CH_2Cl_2:hexane (2:1 by vol) as eluent. After evaporating the solvent, the residue was recrystallized from hexane-$CHCl_3$ to give pure pyrrole **6**. Yield 226 mg (0.68 mmol, 85%); mp 56–58°C; IR (NaCl, film): $\bar{\nu} = 3055$, 2987, 2686, 1602, 1422, 1265, 1156, 896, 705 cm^{-1}; ^1H NMR: $\delta = 0.24$ (s, 9H), 1.34 (m, 2H), 1.54 (m, 2H), 1.66 (m, 2H), 2.25 (s, 3H), 2.31 (t, $J = 7.5$ Hz, 2H), 2.48 (t, $J = 7.5$ Hz, 2H), 3.66 (s, 3H), 8.87 (brs, 1H), 9.57 (s, 1H) ppm; ^{13}C NMR: $\delta = -0.28$, 8.6, 24.1, 24.7, 28.7, 29.4, 34.0, 51.3, 95.1, 102.4, 118.5, 129.1, 129.2, 131.3, 174.0, 176.9 ppm; GC-MS: m/z (%) = 333 [$M^{+\bullet}$], 232, 218 (100), 172, 144, 89.

Methyl 2-Formyl-3-methyl-5-ethynyl-1H-pyrrole-4-hexanoate (**5a**, $C_{15}H_{19}NO_3$)

To a solution of 550 mg (1.65 mmol) of pyrrole **6a** in 12 cm^3 of *THF* was added 1.6 cm^3 of a 1.0 *M* *THF* solution of Bu_4NF. The mixture was stirred at room temperature for 1 h and the color became deeper. After removal of the solvent under reduced pressure, the residue was passed through a short column of silica gel using CH_2Cl_2:hexane (3:1 by vol) as eluent to give a yellow solution. After evaporation of the solvent, a yellow solid was obtained. Yield 310 mg (1.187 mmol, 72%); mp 70–72°C; IR (NaCl, CH_2Cl_2): $\bar{\nu} = 3430$, 3055, 2940, 1732, 1646, 1445, 1264, 896, 604 cm^{-1}; ^1H NMR: $\delta = 1.37$ (m, 2H), 1.53 (m, 2H), 1.65 (m, 2H), 2.26 (s, 3H), 2.30 (t, $J = 7.8$ Hz, 2H), 2.49 (t, $J = 7.5$ Hz, 2H), 3.42 (s, 1H), 3.66 (s, 3H), 9.17 (brs, 1H), 9.59 (s, 1H) ppm; ^{13}C NMR: $\delta = 8.5$, 24.0, 24.6, 28.6, 29.5, 33.9, 51.3, 74.5, 84.0, 117.4, 129.32, 129.37, 131.5, 174.1, 177.1 ppm; GC-MS: m/z (%) = 261 [$M^{+\bullet}$], 230, 188, 174, 146 (100), 117, 91, 65.

1,4-Bis[methyl 4-methyl-5-formyl-2-pyrrolyl-3-hexanoate]butadiyne (**3a**, $C_{24}H_{24}N_2O_6$)

To a solution of 13.26 mg (0.0118 mmol) of tetrakis(triphenyphosphine)palladium(0), 7.88 mg (0.043 mmol) of copper(I) iodide, and 0.16 cm^3 (1.15 mmol) of dry triethylamine in 7.4 cm^3 of dry benzene was added a mixture of 150 mg (0.57 mmol) of pyrrole **5a** and 0.044 cm^3 (0.57 mmol) of chloroacetone in 3.7 cm^3 of dry benzene in one portion. The black mixture was stirred at room temperature for 20 h. After the solvent was evaporated, the residue was passed through a silica gel column using chloroform as eluent. The eluted product was further purified through radial chromatography and recrystallized from ethyl acetate to afford yellow crystals. Yield 96.8 mg (0.186 mmol, 65%); mp 156–158°C. IR (NaCl, film): $\bar{\nu} = 3421$, 3055, 2987, 1725, 1643, 1422, 1265, 1156, 896, 740 cm^{-1}; ^1H NMR: $\delta = 1.34$ (m, 4H), 1.57 (m, 4H), 1.71 (m, 4H), 2.28 (s, 6H), 2.34 (t, $J = 7.65$ Hz,

4H), 2.53 (t, $J = 7.35$ Hz, 4H), 3.69 (s, 6H), 9.34 (brs, 2H), 9.62 (s, 1H) ppm; ^{13}C NMR: $\delta = 8.6$, 23.9, 24.5, 28.4, 29.5, 34.0, 51.6, 75.2, 80.3, 116.9, 129.1, 130.2, 133.9, 174.3, 177.2 ppm.

1,4-Bis[methyl 4-methyl-5-formyl-2-pyrrolyl-3-propanoate]butadiyne (**3b**, $C_{24}H_{24}N_2O_6$)

Dipyrrole **3b** was prepared as described for **3a** (above), using **5b** [33] as starting material. Yield 81 mg (0.18 mmol, 64%); mp 214–216°C; IR (KBr, film): $\bar{\nu} = 3424$, 3299, 2922, 2804, 1722, 1645, 1443, 1379, 1229, 1168, 986, 866, 719 cm^{-1}; ^{1}H NMR: $\delta = 2.30$ (s, 6H), 2.59 (t, $J = 7.5$ Hz, 4H), 2.86 (t, $J = 7.5$ Hz, 4H), 3.69 (s, 6H), 9.44 (brs, 2H), 9.62 (s, 2H) ppm; ^{13}C NMR: $\delta = 8.5$, 19.9, 34.1, 51.7, 74.75, 80.5, 116.8, 129.4, 130.2, 131.8, 173.0, 177.3 ppm.

2,2′-(1,4-Diethyndiyl)bis[[(Z,Z)-5-(3-ethyl-1,5-dihydro-4-methyl-5-oxo-2H-pyrrole-2-ylidene)methyl]-4-methyl-1H-pyrrole-3-hexanoic acid] (**1a**, $C_{42}H_{50}N_4O_6$)

To a solution of 64 mg (0.12 mmol) of dipyrrole dialdehyde **3a**, 67.5 mg (0.48 mmol, 4 mol equiv) of tosyl lactam **4**, and 0.12 cm^3 (0.96 mmol) of tri-*n*-butylphosphine in 3.2 cm^3 of anhydrous *THF* was added a solution of 0.072 cm^3 (0.48 mmol, 4 mol equiv) of *DBU* in 1 cm^3 of anhydrous *THF* in one portion under N_2. The mixture was stirred at room temperature for 24 h; then all the solvents were removed under vacuum. The residue was eluted through a short column of silica gel using hexane first and then ethyl acetate:CH_2Cl_2 (from 1:3 to gradually 1:1 by vol). The yellow eluent was collected and evaporated to dryness. The residue, which was comprised mainly of tetrapyrrole diester **2a**, was used directly in the next step.

To the solution of dimethyl ester **2a** in 15 cm^3 of ethanol (N_2-saturated) was added nitrogen saturated 9 cm^3 of 2 *N* sodium hydroxide solution, and the mixture was heated at reflux under N_2 in the dark for 3 h. The ethanol was then evaporated, and the residue was diluted with cold 25 cm^3 of H_2O and kept at 0°C for 2 h. The precipitate, which was the sodium salt of rubin **1a**, was collected by filtration and washed with cold water. It was re-dissolved in a mixture of 20 cm^3 (10:1 by vol) of H_2O:ethanol using a hot water-bath and then cooled to room temperature and acidified carefully with HO*Ac*. The resulting red precipitate was collected by filtration and washed with cold H_2O to afford acid **1a** as a red solid. Yield 35 mg (0.048 mmol, 40%); mp 288°C (dec); IR (KBr, film): $\bar{\nu} = 3415$, 3309, 2924, 2362, 1662, 1632, 1465, 1389, 1261, 1171, 675 cm^{-1}; ^{1}H NMR (*DMSO*-d_6, 500 MHz): $\delta = 1.09$ (t, $J = 7.5$ Hz, 6H), 1.30 (t, $J = 7.0$ Hz, 4H), 1.48 (t, $J = 7.75$ Hz, 4H), 1.52 (t, $J = 7.5$ Hz, 4H), 1.80 (s, 6H), 2.08 (s, 6H), 2.20 (t, $J = 7.25$ Hz, 4H), 2.45 (t, $J = 7.25$ Hz, 4H), 2.51 (q, $J = 7.5$ Hz, 4H), 5.93 (s, 2H), 9.91 (brs, 2H), 11.17 (brs, 2H), 11.96 (brs, 2H) ppm; ^{13}C NMR (*DMSO*-d_6, 500 MHz): $\delta = 8.1$, 9.1, 14.6, 17.0, 24.3, 28.2, 29.7, 30.6, 33.6, 78.2, 80.1, 95.7, 112.1, 121.5, 124.8, 126.8, 131.6, 132.8, 147.3, 172.1, 174.4 ppm.

10,10a,10b,10c-Tetradehydro-10a,10b,10c-trishomomesobilirubin-XIIIα Dimethyl Ester (**2b**, $C_{38}H_{54}N_4O_6$)

To a solution of 1.5 mmol of tosyl lactam **4**, 218.3 mg (0.5 mmol) of dipyrrole-dialdehyde **3b**, and 0.75 mmol of tri-*n*-butylphosphine in 15 cm^3 of anhydrous *THF* was added a solution of 0.21 cm^3 of *DBU* in 2.5 cm^3 of anhydrous *THF* in one portion under N_2. The mixture was stirred at room temperature for 24 h after which all solvent was removed under vacuum. The residue was eluted through a short column of silica gel, first with hexane and then with ethyl acetate:CH_2Cl_2 (from 1:3 to gradually 1:1 by vol). After evaporation of the pure fractions, the product was recrystallized from hot ethyl acetate to give **2b**. Yield 162 mg (0.25 mmol, 56%); mp 340°C (dec), IR (KBr, film): $\bar{\nu} = 3314$, 2966, 2359, 1739, 1660, 1438, 1386, 1261, 1165, 768 cm^{-1}; ^{1}H NMR (*DMSO*-d_6): $\delta = 1.05$ (t, $J = 7.05$ Hz, 6H), 1.76 (s, 6H), 2.02 (s, 6H), 2.46 (t, $J = 7.5$ Hz, 4H), 2.49 (q, $J = 7.05$ Hz, 4H), 2.70 (t, $J = 7.5$ Hz, 4H), 3.52 (s, 6H), 5.89 (s, 2H), 9.86 (brs, 2H), 11.20 (brs, 2H) ppm; ^{13}C NMR:

$\delta = 8.5$, 9.4, 15.1, 17.5, 20.7, 34.5, 51.8, 78.3, 80.7, 95.9, 112.4, 122.0, 125.4, 127.4, 131.3, 132.3, 147.8, 172.6, 172.8 ppm; FAB (3-*NBA* matrix)-HRMS: calcd. [$M^{+\bullet}$] for $C_{38}H_{42}N_4O_6$: 650.3104, found: 650.3116.

10,10a,10b,10c-Tetradehydro-10,10b,10c-trishomomesobilirubin-XIIIα
(**1b**, $C_{36}H_{38}N_4O_6$)

To a solution of 10.4 mg (0.016 mmol) of tetrapyrrole diester **2b** in 5 cm^3 of N_2-saturated ethanol was added 3 cm^3 of N_2-saturated 2 *N* sodium hydroxide solution, and the mixture was heated at reflux under N_2 in the dark for 3 h. The ethanol was evaporated, and the residue was diluted with 10 cm^3 of cold H_2O and kept at 0°C for 2 h. The resulting precipitate, the sodium salt of rubin **1b**, was collected by filtration and washed with ether. It was dissolved in 10 cm^3 of hot H_2O, then cooled to room temperature and acidified carefully with HO*Ac*. The resulting red precipitate was collected by filtration and washed with cold H_2O to afford acid **1b** as a red solid. Yield 7 mg (60%); mp 400°C (dec); IR (KBr, film): $\bar{\nu} = 3423$, 3304, 2929, 1845, 1652, 1559, 1387, 1251, 1168, 671 cm^{-1}; ^{1}H NMR (*DMSO*-d_6, 500 MHz): $\delta = 1.05$ (t, $J = 7.2$ Hz, 6H), 1.76 (s, 6H), 2.02 (s, 6H), 2.40 (t, $J = 7.5$ Hz, 4H), 2.49 (q, $J = 7.2$ Hz, 4H), 2.66 (t, $J = 7.2$ Hz, 4H), 5.89 (s, 2H), 9.86 (brs, 2H), 11.19 (brs, 2H), 12.07 (brs, 2H) ppm; ^{13}C NMR (*DMSO*-d_6, 500 MHz): $\delta = 8.5$, 9.4, 15.1, 17.5, 20.8, 34.8, 78.4, 80.8, 96.0, 112.4, 122.1, 125.3, 127.3, 131.6, 132.3, 147.8, 172.6, 174.0 ppm; FAB (3-*NBA* matrix)-HRMS: calcd. [$M^{+\bullet}$] for $C_{36}H_{38}N_4O_6$: 622.2746, found: 622.2729.

Acknowledgment

We thank the National Institutes of Health (HD-17779) for generous support of this work.

References

[1] Chowdhury JR, Wolkoff AW, Chowdhury NR, Arias IM (2001) Hereditary Jaundice and Disorders of Bilirubin Metabolism. In: Scriver CF, Beaudet AL, Sly WS, Valle D (eds) The Metabolic and Molecular Bases of Inherited Disease, chap 125. McGraw-Hill, New York, pp 3063–3101

[2] a) McDonagh AF (1979) Bile Pigments: Bilatrienes and 5,15-Biladienes. In: Dolphin D (ed) The Porphyrins, vol VI, chap 6. Academic Press, New York; b) Schmid R, McDonagh AF (1979) Hyperbilirubinemia. In: Stanbury JB, Wyngaarden JB, Fredrickson DS (eds) The Metabolic Basis of Inherited Disease, 4th ed. McGraw-Hill, New York, pp 1221–1257

[3] Falk H (1989) The Chemistry of Linear Oligopyrroles and Bile Pigments. Springer-Verlag, Wien

[4] Fischer H, Plieninger H (1942) Hoppe-Seyler's Z Physiol Chem **274**: 231

[5] Lemberg R (1939) Austral Chem Int J and Proc **6**: 170

[6] Lemberg R, Legge JW (1949) Hematin Compounds and Bile Pigments. Interscience Publ, New York

[7] a) Falk H, Gergeley S, Grubmayr K (1976) Monatsh **107**: 827; b) Falk H, Gergeley S, Grubmayr K, Hofer O (1977) Liebigs Ann Chem 565; c) Falk H, Müller X (1985) Org Magn Reson **23**: 353

[8] a) Sheldrick WS (1983) Israel J Chem **23**: 155; b) Sheldrick WS (1976) J Chem Soc Perkin 2: 1457; c) Bonnett R, Davies JE, Hursthouse NB, Sheldrick GM (1978) Proc R Soc London, Ser B **202**: 249; d) LeBas G, Allegret A, Mauguen Y, DeRango C, Bailly M (1980) Acta Crystallogr Sect B **B36**: 3007; e) Becker W, Sheldrick WS (1978) Acta Crystallogr Sect B **B34**: 1298

[9] Person RV, Peterson BR, Lightner DA (1994) J Am Chem Soc **116**: 42

[10] a) Chen Q-Q, Ma J-S, Wang C-Q, Liu Y-Y, Yan F, Cheng L-J, Jin S, Falk H (1995) Monatsh Chem **126**: 983; b) Chen Q-Q, Falk H (1995) Monatsh Chem **126**: 1097

[11] Pfeiffer WP, Lightner DA (1994) Tetrahedron Lett **35**: 9673

[12] Tu B, Lightner DA (2003) J Heterocyclic Chem **32**: 707
[13] Boiadjiev SE, Lightner DA (1994) SYNLETT: 777
[14] Chen Q, Huggins MT, Lightner DA, Norona W, McDonagh AF (1999) J Am Chem Soc **121**: 9253
[15] Kar A, Lightner DA (1998) Tetrahedron **54**: 5151
[16] Trull FR, Franklin RW, Lightner DA (1987) J Heterocyclic Chem **24**: 1573
[17] a) Bobál P, Lightner DA (2001) J Heterocyclic Chem: 1219; b) Thyrann T, Lightner DA (1996) Tetrahedron Lett **37**: 315
[18] Sonogashira K, Tohda Y, Hagihara N (1975) Tetrahedron Lett 4467
[19] Brower JO, Lightner DA, McDonagh AF (2000) Tetrahedron **56**: 7869
[20] a) Lightner DA, Person RV, Peterson BR, Puzicha G, Pu Y-M, Bojadziev S (1991) Biomolecular Spectroscopy II. In: Birge RR, Nafie LA (eds) Proc SPIE 1432: 2; b) Shrout DP, Puzicha G, Lightner DA (1992) Synthesis: 328; c) Trull FR, Person RV, Lightner DA (1997) J Chem Soc Perkin Trans **2**: 1241
[21] Dörner T, Knipp B, Lightner DA (1997) Tetrahedron **53**: 2697
[22] a) Nogales D, Lightner DA (1995) J Biol Chem **270**: 73; b) Lightner DA, Wooldridge TA, Rodgers SL, Norris RD (1980) Experientia **36**: 380
[23] a) Boiadjiev SE, Anstine DT, Lightner DA (1995) J Am Chem Soc **117**: 8727; b) Boiadjiev SE, Anstine DT, Maverick E, Lightner DA (1995) Tetrahedron: Asymm **6**: 2253
[24] a) Huggins MT, Lightner DA (2000) J Org Chem **65**: 6001; (b) Huggins MT, Lightner DA (2001) Tetrahedron **57**: 2279
[25] (a) Huggins MT, Lightner DA (2001) Monatsh Chem **132**: 203; (b) Nogales DF, Ma J-S, Lightner DA (1993) Tetrahedron **49**: 2361
[26] a) Brower JO, Huggins MT, Boiadjiev SE, Lightner DA (2000) Monatsh Chem **131**: 1047; b) Huggins MT, Lightner DA (2001) Monatsh Chem **132**: 203
[27] Molecular Mechanics and Dynamics Calculations Employed to find the Global Energy Minimum Conformations of **1** were Run on an SGI Octane Workstation using vers. 6.9 of the Sybyl Forcefield as Described in refs. 9 and 33; for the Ball and Stick Drawings were Created from the Atomic Coordinates using Müller and Falk's ''Ball and Stick'' Program for the Macintosh (http://www.orc.uni-Linz.ac.at/mueller/ball_and_stick.shtml)
[28] Lightner DA, Gawroński JK, Wijekoon WMD (1987) J Am Chem Soc **109**: 6354
[29] (a) Falk H, Vormayr G, Margulies L, Metz S, Mazur Y (1986) Monatsh Chem **117**: 849; (b) Falk H, Grubmayr K, Höllbacher G, Hofer O, Leodolter A, Neufingerl F, Ribó JM (1977) Monatsh Chem **108**: 1113
[30] Kasha M, El-Bayoumi MA, Rhodes W (1961) J Chim Phys-Chim Biol **58**: 916
[31] Harada N, Nakanishi K (1983) Circular Dichroic Spectroscopy-Exciton Coupling in Organic Stereochemistry. University Science Books, Mill Valley, CA
[32] (a) Lightner DA, Reisinger M, Landen GL (1986) J Biol Chem **261**: 6034; (b) McDonagh AF, Lightner DA (1988) Seminars in Liver Disease **8**: 272; (c) Boiadjiev SE, Lightner DA (1999) Tetrahedron: Asymmetry **10**: 607
[33] Tu B, Ghosh B, Lightner D (2003) J Org Chem **68**: 8950
[34] Sheu JH, Yen CF, Huang HC, Huang HLV (1989) J Org Chem **54**: 5126